Numerical Simulation of Local Flow-Field Characteristics in the Sand–Gravel Transition Zone under Localized Leakage

Jiahui Liang[1,2], Chen Peng[3], Meng Yang[1,2,*], Yu Jia[1,2], Lei Tang[1,2], Pinzhi Luan[1,2]
[1]*Materials & Structural Engineering Department, Nanjing Hydraulic Research Institute, Nanjing, Jiangsu, China*
[2]*The National Key Laboratory of Water Disaster Prevention, Nanjing, Jiangsu, China*
[3]*Dayu College, Hohai University, Nanjing, Jiangsu, China*
**Corresponding Author*

Abstract: Local leakage in asphalt concrete core walls is usually highly concealed, and its influence on the downstream transition materials is difficult to characterize directly. To reveal the flow-field response of the sand–gravel transition zone under localized leakage in the core wall, a three-dimensional equivalent seepage model of the downstream sand–gravel transition zone was established. The local velocity field, pressure field, velocity head, and velocity distributions along two virtual survey lines were analyzed under concentrated leakage conditions. The results show that a localized leakage inlet can generate a flow field with clear spatial directivity in the downstream sand–gravel transition zone. The high-velocity region is concentrated near the leakage inlet and spreads along the dominant seepage direction, while the pressure decreases continuously along the seepage path. Along the elevation direction, the high-velocity zone occurs near the elevation range affected by the leakage inlet, with the velocity decreasing gradually toward lower elevations. Along the dam-axis direction, the velocity distribution exhibits higher values in the central region and lower values on both sides, and the peak position corresponds well to the projection of the leakage inlet. These findings indicate that the leakage-driven flow field in the sand–gravel transition zone exhibits identifiable spatial response characteristics, which can provide a basis for understanding local seepage mechanisms and arranging subsequent monitoring sections.

Keywords: Asphalt Concrete Core Wall; Sand–Gravel Transition Zone; Localized Leakage; Local Seepage Field; Virtual Survey Line; Spatial Response

1. Introduction

Asphalt concrete core rockfill dams have been widely used in high earth–rockfill dam projects because of their excellent seepage-control performance, strong deformation adaptability, and high construction efficiency [1–3]. The core wall is the key component of the dam seepage-control system, and its integrity is directly related to the seepage safety of the dam. Recent studies have shown that differences in material stiffness and deformation compatibility exist between the asphalt concrete core wall and the adjacent transition materials. Under the combined effects of reservoir impoundment, settlement, and seepage, shear deformation, local damage, or potential leakage may occur at the interface between the core wall and the transition zone [4–6]. Therefore, understanding the seepage response induced by local leakage in asphalt concrete core wall dams is an important issue in dam safety assessment.

A certain degree of seepage generally exists during the operation of earth–rockfill dams. However, concentrated leakage and the associated internal erosion can significantly threaten dam safety. Recent review studies have indicated that seepage control, anomaly detection, and defect treatment are essential for the safe operation of earth–rockfill dams, and that a single detection method is often insufficient to fully identify complex leakage pathways [7]. The sand–gravel transition zone is located between the core wall and the rockfill shell. It functions as a filter and transition layer, and also serves as a main flow path through which leakage water enters the downstream region after local leakage occurs in the core wall. Therefore, investigating the spatial response of the internal velocity field in the sand–gravel transition zone under localized leakage is of great significance for understanding the development mechanism of concealed seepage in asphalt concrete core wall dams.

At present, dam leakage detection methods mainly include piezometric monitoring, drainage discharge analysis, tracer tests, temperature-field monitoring, electrical methods, infrared thermography, borehole inspection, and in-borehole observation [7–13]. Among these methods, natural tracers such as temperature and electrical conductivity can be used to identify seepage anomalies [8]. Distributed fiber-optic temperature sensing can provide temperature responses with relatively high spatial resolution [9,10]. Electrical resistivity tomography can infer internal defects or leakage paths from electrical anomalies [11,13]. Infrared thermography can identify leakage zones from surface temperature differences [12]. These methods provide important tools for detecting seepage anomalies. However, in complex dam structures, their interpretations may still be affected by non-uniqueness, material heterogeneity, and site-dependent boundary conditions.

For asphalt concrete core wall dams, engineering investigations commonly combine boreholes, sonar detection, borehole TV inspection, tracer tests, water-level analysis, and geophysical methods to evaluate leakage conditions and infer leakage paths [3,7]. Existing studies have mainly focused on leakage anomaly detection and leakage-channel exploration. However, targeted analyses remain limited regarding how a localized leakage point controls the velocity distribution in the downstream sand–gravel transition zone and how the velocity peak, high-velocity zone, and attenuation trend respond to the spatial position of the leakage inlet. It is therefore necessary to investigate the relationship between localized leakage and downstream flow-field response from the perspective of local seepage-field mechanisms.

Theoretically, low-velocity steady seepage in the sand–gravel transition zone can be described by Darcy’s law. At the engineering scale, sand–gravel materials are commonly treated as equivalent continuous porous media, and their seepage capacity can be characterized by hydraulic conductivity or intrinsic permeability [14–16]. The Kozeny–Carman relationship is a widely used empirical model for estimating permeability from porosity and representative particle size, although its predictions may be affected by pore-scale heterogeneity and particle-structure variations [15,16]. These theories provide a basis for constructing an equivalent seepage model and analyzing the macroscopic flow-field response in sand–gravel materials.

Based on the above considerations, this study focuses on local leakage in an asphalt concrete core wall and establishes a three-dimensional equivalent seepage model for the downstream sand–gravel transition zone. The local velocity field, pressure field, velocity head, and velocity distribution along virtual survey lines driven by localized leakage are investigated. By analyzing velocity peaks, high-velocity zones, and attenuation trends along the elevation and dam-axis directions, the controlling effect of localized leakage on the downstream flow field in the sand–gravel material is revealed. The results are expected to provide a theoretical basis for understanding leakage-induced flow-field evolution and optimizing subsequent monitoring layouts.

2. Local Seepage Model under Core-Wall Leakage

2.1 Numerical Model Development

When local defects occur in the asphalt concrete core wall, leakage water may enter the downstream sand–gravel transition zone through a concentrated flow path and form a local seepage field controlled by the leakage point. To simulate this seepage field appropriately, the hydraulic characteristics of the sand–gravel transition zone need to be reasonably described. However, sand–gravel materials have complex particle compositions. Although a particle-based random packing model can represent local pore structures, it usually leads to complicated geometric boundaries, a large number of mesh elements, and low computational efficiency. Since this study focuses on the overall velocity distribution controlled by the leakage point rather than pore-scale local flow, the sand–gravel transition zone is treated as an equivalent continuous porous medium, and its seepage behavior is characterized by macroscopic parameters such as porosity and permeability [14–16].

A three-dimensional local seepage model was established to represent the sand–gravel transition zone downstream of the core wall. The model dimensions were 1500 mm × 1000 mm ×

1000 mm. The coordinate system was defined as follows: the X-axis represents the upstream–downstream direction, the Y-axis represents the dam-axis direction, and the Z-axis represents the elevation direction.

2.2 Governing Equations and Parameter Settings

The seepage flow in the sand–gravel transition zone can be regarded as low-velocity steady flow in a saturated porous medium. Based on Darcy's law, the relationship between seepage velocity and hydraulic gradient is expressed as [14]:

$$v=-K\nabla h \tag{1}$$

where v is the Darcy seepage velocity vector, K is the hydraulic conductivity, h is the total hydraulic head, and ∇h is the hydraulic gradient. When expressed in terms of intrinsic permeability, the Darcy velocity can be written as:

$$u=-\frac{k}{\mu}\nabla p \tag{2}$$

where u is the Darcy velocity, k is the intrinsic permeability of the porous medium, μ is the dynamic viscosity of the fluid, and p is the pore-water pressure. Water was assumed to be incompressible, and the dynamic viscosity was taken as 1.0×10^{-3} Pa·s.

The permeability of the sand–gravel material was estimated using the Kozeny–Carman model [15,16]:

$$k=\frac{d_p^2 n^3}{180(1-n)^2} \tag{3}$$

where d_p is the representative particle size and n is the porosity. In this study, d_p=10 mm and n=0.3. The sand–gravel transition zone was assumed to be a homogeneous and isotropic saturated porous medium. The leakage path was simplified as a stable concentrated inflow boundary. Heterogeneity, non-Darcy flow, and the coupling effects of multiple leakage points were not considered at this stage.

2.3 Geometry and Boundary Conditions

To simulate the concentrated leakage path caused by a local defect in the core wall, a 100 mm × 100 mm rectangular inflow boundary was assigned on the upstream side of the model, as shown in Figure 1(a). A normal inflow velocity of 0.05 m/s was applied at the inlet. A pressure outlet was set on the downstream side, as shown in Figure 1(b), with the pressure specified as 0 Pa. The remaining boundaries were treated as no-flow or symmetry boundaries, so that seepage mainly developed from the inlet toward the outlet. Gravity was included in the calculation to account for the influence of elevation on the hydraulic head distribution.

As shown in Figure 1(c), the model was discretized using free tetrahedral elements with physics-controlled meshing. Considering the relatively large velocity gradient near the inlet, a refined mesh level was adopted. The final model contained 153,723 degrees of freedom. A steady-state solution was then obtained to derive the Darcy velocity field, pressure field, and velocity head distribution, which served as the basis for the subsequent analysis of flow-velocity responses.

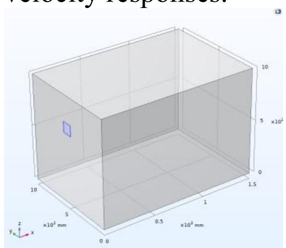

(a) Inlet of the Local Leakage Model

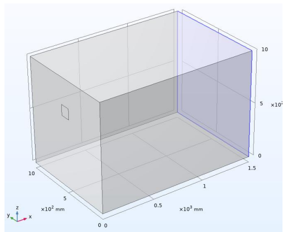

(b) Outlet of the Local Leakage Model

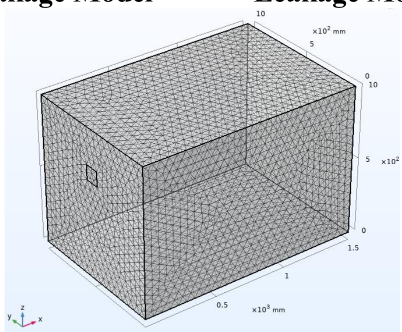

(c) Schematic Diagram of Mesh Generation

Figure 1. Local Seepage Model

2.4 Arrangement of Virtual Survey Lines

To investigate the influence of localized leakage on the velocity distribution in different directions, two orthogonal virtual survey lines were arranged in the model. The first survey line was aligned with the center of the leakage outlet and extended along the elevation direction, with endpoints at (500, 500, 1000) and (500, 500, 0). This line was used to extract Darcy velocities at different elevations and to characterize the elevation-dependent velocity response under localized leakage.

The second survey line was arranged along the dam-axis direction, with endpoints at (500, 0, 500) and (500, 1000, 500), and was located at the elevation of Z = 500 mm. This line was used to extract velocity data at different dam-axis positions under the same elevation condition and to analyze the lateral diffusion and attenuation characteristics of the leakage-driven flow field.

3. Leakage-Driven Flow-Field Distribution Characteristics

3.1 Seepage-Field Characteristics

As shown in Figure 2, after the leakage water enters the sand–gravel transition zone through the local inflow boundary, a local seepage field with a clear spatial orientation is formed downstream. The three-dimensional frame in Figure 2 follows the model coordinate system defined above: the X-axis represents the upstream–downstream direction, the Y-axis represents the dam-axis direction, and the Z-axis represents the elevation direction. The streamlines describe the main seepage paths after water enters from the local inflow boundary, while the color bar represents the magnitude of the total Darcy velocity in m/s. Because the color scale is marked by $\times10^{-2}$, larger values on the bar correspond to higher velocity magnitudes near the leakage inlet. The high-velocity region is mainly concentrated near the leakage inlet and then spreads along the dominant seepage direction. As the measuring points move farther away from the leakage inlet, the hydraulic gradient decreases, and the Darcy velocity gradually declines.

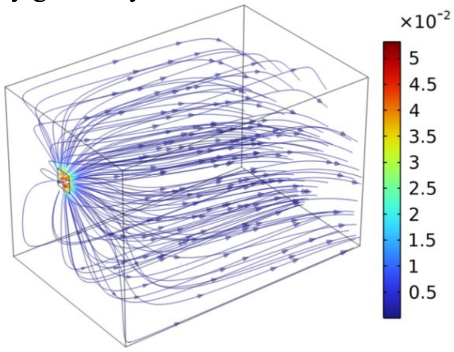

Figure 2. Total Darcy Velocity Field of Local Seepage (m/s)

As shown in Figure 3, the pressure field also reflects the controlling effect of the leakage point on the flow field. Figure 3(a), Figure 3(b), and Figure 3(c) present the pressure distributions on the YZ, XY, and XZ planes, respectively, thereby describing the pressure variation from different sectional views of the same three-dimensional seepage domain. In each subfigure, the color bar denotes the pore-water pressure in Pa; higher values on the color scale indicate higher pressure, while lower values indicate pressure attenuation along the seepage path. It should be noted that the color ranges of different sectional plots are used to show the pressure variation within each plane, so the spatial gradient and relative distribution pattern are more important than a direct comparison of colors between different planes. The pressure is relatively high near the inlet and gradually decreases along the seepage path, forming a continuous hydraulic-head gradient. The spatial variation of the velocity field is consistent with that of the pressure field; that is, regions with larger hydraulic gradients correspond to higher Darcy velocities, which agrees with the theory of steady seepage flow [14]. Therefore, the velocity peak, attenuation trend, and spatial distribution characteristics at different downstream locations can be used as key descriptors of the leakage-driven local flow-field response.

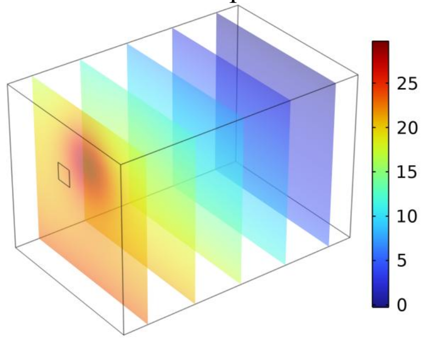

(a) Pressure Field in the YZ Plane

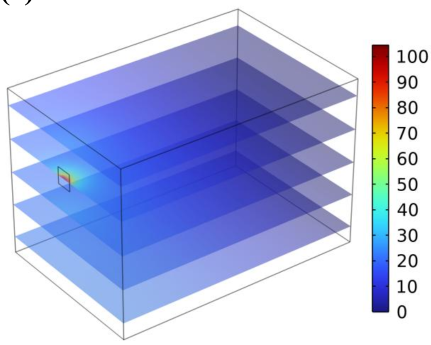

(b) Pressure Field in the XY Plane

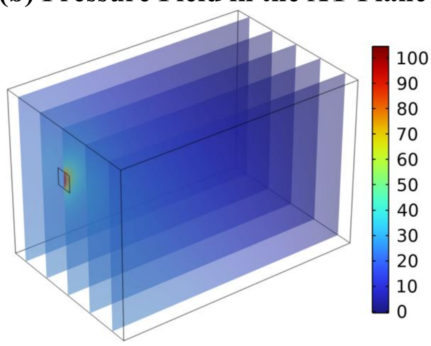

(c) Pressure Field in the XZ Plane

Figure 3. Pressure Field of Local Seepage (Pa)

3.2 Velocity Response Characteristics along the Virtual Survey Lines

The velocity-head distribution along the elevation-direction virtual survey line is shown in Figure 4(a). In Figure 4, the horizontal axis represents the coordinate along the elevation-direction virtual survey line, expressed by the elevation coordinate Z in mm. The vertical axis in Figure 4(a) represents the velocity head in mm, whereas the vertical axis in Figure 4(b) represents the total Darcy velocity in mm/s. Using the same horizontal coordinate in the two subfigures makes it possible to compare the variation in hydraulic head and velocity along the same survey line. The velocity head along this line exhibits a stable seepage pattern and varies continuously along the elevation direction, forming an approximately linear distribution. This relatively uniform hydraulic-head gradient indicates the presence of a steady seepage field in this region, which is consistent with the seepage behavior of porous media described by Darcy's law.

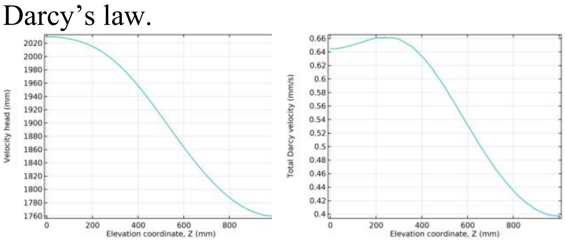

(a) Velocity Head (b) Total Darcy Velocity

Figure 4. Seepage Distribution Characteristics Along the Elevation-Direction Virtual Survey Line

The magnitude of the total Darcy velocity along the elevation-direction virtual survey line is shown in Figure 4(b). Compared with the velocity-head curve in Figure 4(a), the velocity curve more directly reflects the local seepage response along the survey line. The vertical velocity distribution presents typical characteristics induced by leakage. Along the elevation direction, the velocity remains at a relatively high level near Z = 700–900 mm, with a maximum value of approximately 0.660 mm/s. As the measuring points move away from the high-velocity region, the velocity gradually decreases and reaches approximately 0.397 mm/s at the end of the survey line. This distribution indicates that the high-velocity region is associated with the vertical influence range of the leakage inlet, while the decreasing velocity trend reflects the attenuation of the hydraulic gradient. The velocity-head distribution is clearly correlated with the total Darcy velocity distribution. Regions with larger velocity head correspond to higher hydraulic gradients and higher Darcy velocities, indicating that the elevation-direction velocity profile is sensitive to the vertical influence range of localized leakage.

The velocity-head distribution along the dam-axis-direction virtual survey line is shown in Figure 5(a). In Figure 5, the horizontal axis represents the dam-axis coordinate Y in mm. The vertical axis in Figure 5(a) represents the velocity head in mm, and the vertical axis in Figure 5(b) represents the total Darcy velocity in mm/s. The two curves therefore describe the hydraulic-head response and the velocity response along the same horizontal section at Z = 500 mm. The velocity-head distribution exhibits typical radial diffusion characteristics. The velocity head gradually decreases from the central region toward both sides along the dam-axis direction, forming a nearly symmetric distribution centered around the local inflow boundary. This pattern indicates the presence of a concentrated leakage effect near the central region.

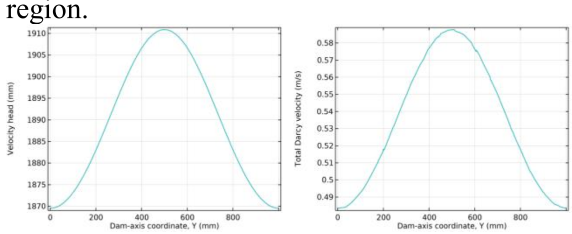

(a) Velocity head (b) Total Darcy velocity

Figure 5. Seepage Distribution Characteristics along the Dam-Axis-Direction Virtual Survey Line

As shown in Figure 5(b), the total Darcy velocity exhibits a distinct peak near the center of the dam-axis direction, reaching approximately 0.587 mm/s, and then gradually decreases toward both sides to approximately 0.483 mm/s. This distribution reflects the lateral influence range of the localized leakage. The velocity peak appears near the center of the dam-axis direction, indicating that the imposed localized leakage produces a lateral flow response with a clear central high-value region and attenuation toward both sides. The nearly symmetric shape of the curve also suggests that, under the present homogeneous and isotropic assumption, the seepage response along the dam-axis direction is mainly controlled by the distance from the local inflow boundary. Overall, the velocity-head distribution and the Darcy velocity distribution show consistent variation trends. Regions with larger velocity head coincide with regions of higher Darcy velocity, and both exhibit a nearly symmetric distribution centered around the local inflow boundary.

4. Applicability and Future Work

The results of this study are based on an idealized numerical model. In the model, the sand–gravel transition zone is treated as a homogeneous and isotropic porous medium, and only a single localized leakage inlet is considered. Factors such as the heterogeneity of transition materials, variation in gradation and compaction state, non-Darcy flow, and the superposition of multiple leakage paths have not yet been incorporated. Therefore, the present results should be interpreted as a preliminary analysis of leakage-driven flow-field response under simplified conditions.

The main significance of this study lies in demonstrating that localized leakage can produce identifiable spatial response characteristics in the downstream sand–gravel transition zone. The velocity peak, high-velocity region, and attenuation trend along different directions provide useful indicators for understanding the influence range and directional characteristics of local seepage. These response characteristics can help guide the arrangement of monitoring sections or survey lines in subsequent studies, but they should not be directly interpreted as field-scale leakage diagnosis results.

Future work should focus on improving the representativeness of the numerical model and evaluating the robustness of the observed response patterns. First, different leakage elevations, leakage intensities, and inflow boundary sizes should be considered to examine how the velocity peak and high-velocity region vary with leakage conditions. Second, the effects of porosity, permeability, gradation, and spatial heterogeneity of the sand–gravel transition zone should be investigated. Third, laboratory model tests or field monitoring data should be introduced to verify whether the velocity response patterns obtained from the idealized model can be observed under more realistic conditions. In addition, multiple leakage paths and transient seepage conditions should be considered in future analyses to extend the applicability of the proposed flow-field response framework.

5. Conclusions

A three-dimensional equivalent seepage model of the sand–gravel transition zone was established to investigate the local flow-field response under concentrated leakage from an asphalt concrete core wall. The main conclusions are as follows.

(1) Localized leakage forms a seepage field with clear spatial directivity in the downstream sand–gravel transition zone. The high-velocity region is mainly concentrated near the local inflow boundary and spreads along the dominant seepage direction. As the distance from the leakage inlet increases, the hydraulic gradient decreases and the Darcy velocity gradually attenuates.

(2) The pressure field shows a continuous decrease along the seepage path, and its spatial distribution is consistent with the Darcy velocity field. Regions with higher hydraulic gradients correspond to higher Darcy velocities, indicating that the pressure field and velocity field jointly reflect the controlling effect of localized leakage on the surrounding flow field.

(3) Along the elevation-direction virtual survey line, the velocity remains relatively high within the elevation range affected by the leakage inlet, with a maximum value of approximately 0.660 mm/s, and then gradually decreases toward lower elevations. This indicates that the elevation-direction velocity profile can reflect the vertical influence range of localized leakage.

(4) Along the dam-axis-direction virtual survey line, the velocity distribution at the same elevation shows higher values in the central region and lower values on both sides. The peak appears near Y = 499.93 mm, with a maximum value of approximately 0.588 mm/s, indicating that localized leakage produces a lateral flow response characterized by a central peak and attenuation toward both sides.

Overall, the leakage-driven local flow field in the sand–gravel transition zone exhibits identifiable spatial response characteristics. These findings provide a basis for understanding the seepage response mechanism of asphalt concrete core wall leakage and for designing subsequent monitoring layouts.

Acknowledgments

This work was supported by the National Key Research and Development Program of China (Grant No. 2024YFC3214903); the Jiangsu

Province Youth Science and Technology Talent Support Program (Grant No. JSTJ-2025-171); the Postgraduate Thesis Fund of Nanjing Hydraulic Research Institute (Yy425001).

References

[1] Feng S, Wang W, Hu W, et al. Design and performance of the Quxue asphalt-core rockfill dam. Soils and Foundations, 2020, 60(4): 1036-1049.

[2] ICOLD. Asphalt Concrete Cores for Embankment Dams[M]. ICOLD Bulletin Preprint 179. Paris: International Commission on Large Dams, 2018.

[3] Wei M, Zhou H, Cui D. Research and Application on Seepage Detection and Repair of Anti-Seepage System for Earth-Rockfill Dam with Asphalt Concrete Core. American Journal of Water Science and Engineering, 2018, 4(4): 101-106.

[4] Wen L, Huang J, Yang Y. Shear behavior of the interface between asphalt concrete core and transition under seepage effect. Scientific Reports, 2025, 15: 22660.

[5] Wen L, Cao W, Yang Y, et al. Experimental study on the shear behavior of the interface between asphalt concrete core wall and transition layer. Construction and Building Materials, 2024, 440: 137469.

[6] Zheng X, Yan B, Wang W, Du K, Fang Y. Seepage-Deformation Coupling Analysis of a Core Wall Rockfill Dam Subject to Rapid Fluctuations in the Reservoir Water Level. Water, 2024, 16(11): 1621.

[7] EL-Molla D A, Kilit M. Seepage Control, Detection, and Treatment in Embankment Dams: A State-of-the-Art Review. Arabian Journal for Science and Engineering, 2026, 51: 3823-3849.

[8] Qiu H, Li X, Li Z, et al. Detection and Quantification of Dam Leakages Based on Tracer Tests: A Field Case Study. Water, 2022, 14(9): 1448.

[9] Ghafoori Y, Vidmar A, Riha J, Kryzanowski A. A Review of Measurement Calibration and Interpretation for Seepage Monitoring by Optical Fiber Distributed Temperature Sensors. Sensors, 2020, 20(19): 5696.

[10] Cheng L, Liu H, Wang X, et al. An experimental study on monitoring the phreatic line of an embankment dam based on temperature detection by OFDR. Measurement, 2021, 173: 108609.

[11] Norooz R, Nivorolis A, Olsson P I, et al. Monitoring of Alvkarleby test embankment dam using 3D electrical resistivity tomography for detection of internal defects. Journal of Civil Structural Health Monitoring, 2024, 14(5): 1275-1294.

[12] Zhou R, Su H, Wen Z. Experimental study on leakage detection of grassed earth dam by passive infrared thermography. NDT & E International, 2022, 126: 102583.

[13] Norooz R, Dahlin T, Toromanovic J. Integration of seepage modelling and electrical resistivity monitoring data for the Alvkarleby test embankment dam, Sweden. Engineering Geology, 2025, 357: 108311.

[14] Fu B, Pei J, Ji H. Numerical simulation of three-dimensional seepage field in a tailing pond under multiple operating conditions. Scientific Reports, 2024, 14: 28027.

[15] Zhu J. Uncertainty of Kozeny-Carman Permeability Model for Fractal Heterogeneous Porous Media. Hydrology, 2023, 10(1): 21.

[16] Jiao W, Scheidweiler D, Delouche N, de Anna P, Guadagnini A. Intrinsic permeability of heterogeneous porous media. Physical Review Fluids, 2024, 9: 094102.